Monte Carlo Simulation of the 2D Ising Model: Critical Temperature and Phase Transition Analysis

Solveig Juntunen, Erling Sandbekk
(Dated: November 20, 2025)

We study the two-dimensional ferromagnetic Ising model on square lattices with periodic boundary conditions as a model of temperature-dependent behavior in ferromagnets. Using the analytically solvable 2×2 system with its 16 microstates, we derive closed-form expressions for the energy, magnetization, heat capacity, and susceptibility, and use these results to benchmark our numerical code. We then implement a Metropolis Markov Chain Monte Carlo sampler to compute the energy per spin, absolute magnetization per spin, heat capacity per spin, and susceptibility per spin for larger lattices. For the 2×2 lattice, we find that runs of approximately 10^4 Monte Carlo cycles reproduce the analytical results with relative errors typically below 10^{-3}, while burn-in studies for $L = 20$ indicate that discarding the first $\sim 10^4$ cycles yields equilibrated samples across temperatures and initial conditions.

Energy histograms for $L = 20$ show a narrow distribution at $T = 1.0\,J/k_B$ and a broadened distribution at $T = 2.4\,J/k_B$, reflecting enhanced near-critical fluctuations. From peaks in C_V/N and χ/N for $L = 40, 60, 80$, and 100, we extract pseudo critical temperatures $T_c(L) \approx 2.27$–$2.32\,J/k_B$ and, via finite-size scaling, obtain $T_c(\infty) \approx 2.28\,J/k_B$, within 0.5% of Onsager's exact value $T_c = 2.269\,J/k_B$. Finally, OpenMP parallelization of the temperature loop reduces the runtime from 34.0 s (1 thread) to 6.3 s (6 threads) and 4.9 s (12 threads), corresponding to speedups of 5.4 and 6.9 and efficiencies of 0.90 and 0.58, respectively.

I. INTRODUCTION

The goal of this project is to explore the two dimensional Ising model and use it as a simple example of temperature dependent behavior in ferromagnetic systems. Even though the model only consists of spins that can point either up or down and interact only with their nearest neighbors, it still manages to show important physical phenomena such as spontaneous magnetization and phase transitions. Because of this, the 2D Ising model is often used as a clean testing ground for studying collective behavior in many body systems.

Since the state space of an $L \times L$ lattice grows as 2^{L^2}, it quickly becomes impossible to compute thermodynamic quantities by summing over all possible configurations. For this reason we use a Markov Chain Monte Carlo (MCMC) method, specifically the Metropolis algorithm, to generate representative samples from the Boltzmann distribution. From these samples we can estimate quantities such as the energy per spin, the magnetization per spin, the heat capacity, and the magnetic susceptibility. Throughout the project we also pay attention to important practical aspects of MCMC simulations such as burn in time, convergence, and the affect of thermal fluctuations.

Another objective is to investigate how parallelization can speed up Monte Carlo simulations. Because many parts of the computation (like independent MCMC walkers or independent temperature points) do not depend on each other the problem is well suited for parallel execution. In the final part of the project we measure the speed-up obtained by parallelizing our implementation.

Overall, the project combines statistical physics, numerical methods, and practical programming considerations. By comparing numerical results against analytical expressions for the 2×2 lattice and by analyzing the behavior of larger systems we can gain insight into both the physics of the Ising model and the strengths and weaknesses of Monte Carlo methods.

The remainder of the report is organized as follows. In Section II B we present the analytical results for the 2×2 system used to validate our numerical implementation. Section II C describes the MCMC algorithm, including the treatment of periodic boundary conditions and computation of observables. Section II outlines the numerical experiments, covering burn-in analysis, histogram estimation, and performance considerations. Section III presents results for larger lattice sizes and discusses the finite-size scaling used to estimate the critical temperature in the thermodynamic limit. Finally, Section IV summaries our findings and reflects on limitations and possible extensions of the work.

II. METHODS

In this section we describe how the Ising model was implemented and how the Monte Carlo simulations were carried out. The overall goal was to estimate thermodynamic quantities such as the energy, magnetization, heat capacity, and susceptibility by sampling from the Boltzmann distribution. Because the full configuration space grows exponentially with the number of spins, it is not possible to compute exact averages for larger lattices. Instead we used the Metropolis algorithm to generate a Markov chain of spin configurations that approximate the equilibrium distribution at a given temperature.

The methods section also explains how we handled practical issues such as random initial states, burn-in time, sampling frequency, and averaging. Finally we de-

scribe how the code was parallelized by running several independent Monte Carlo walkers in separate threads and how we measured the resulting speed-up. Overall, the aim of this section is to give a clear overview of how the numerical experiments were performed and why these choices were made.

A. The 2D Ising model

We consider the ferromagnetic Ising model on a two–dimensional square lattice (Figure 1). The lattice has linear size L, giving a total of $N = L^2$ sites. Each site hosts a spin variable $s_i \in \{-1, +1\}$, representing magnetic moments pointing either up or down.

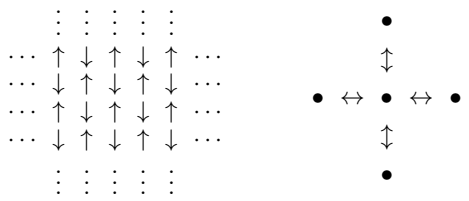

FIG. 1. Basic setup of the two-dimensional Ising model. The square lattice (left) and nearest-neighbor spin interactions (right) are reproduced from [1].

A complete *spin configuration*, or *microstate*, of the system is written as

$$\mathbf{s} = (s_1, s_2, \ldots, s_N).$$

In numerical implementations, this configuration is naturally represented as an $L \times L$ matrix, reflecting the geometry of the lattice. Since each of the N sites can independently assume two spin states, the total number of distinct microstates is

$$|\mathcal{S}| = 2^N.$$

The energy of a configuration $\mathbf{s}$ is is governed by the Hamiltonian

$$E(\mathbf{s}) = -J \sum_{\langle kl \rangle}^{N} s_k s_l \; - \; \mathcal{B} \sum_{k}^{N} s_k, \tag{1}$$

where J is the coupling constant that sets the strength of the spin–spin interaction, and $\mathcal{B}$ denotes an external magnetic field acting on the spins. The notation $\langle kl \rangle$ indicates that the summation is restricted to nearest-neighbor pairs, each counted exactly once.

Choosing $J > 0$ ensures that neighboring spins are energetically favored to be aligned, making the model ferromagnetic. At sufficiently low temperatures, this leads to *spontaneous magnetization*, a cooperative phenomenon in which local magnetic moments give rise to long-range correlations throughout the lattice. Through interactions between nearest neighbors, the orientation of one spin can influence distant spins [2].

To isolate the cooperative effects of spin–spin interactions, we consider the system energy in the absence of an external field ($\mathcal{B} = 0$), which reduces (1) to:

$$E(\mathbf{s}) = -J \sum_{\langle kl \rangle}^{N} s_k s_l. \tag{2}$$

Boundary conditions are particularly significant in finite systems. In this work we adopt *periodic boundary conditions* (PBC), ensuring that each spin interacts with exactly four nearest neighbours—left, right, up, and down—as illustrated in Figure 1. Under PBC, spins located on opposite edges of the lattice are identified as neighbours, rendering the system topologically equivalent to a torus (Figure 2).

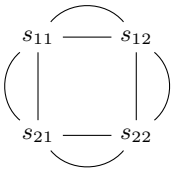

FIG. 2. Periodic boundary conditions in the 2×2 Ising model, giving each spin four neighbours.

For a general $L \times L$ lattice with periodic boundary conditions, the Hamiltonian in Eq. (2) takes the explicit form

$$E(\mathbf{s}) = -J \sum_{i=1}^{L} \sum_{j=1}^{L} \Big(s_{i,j}\, s_{i,j+1} + s_{i,j}\, s_{i+1,j} \Big), \tag{3}$$

with indices taken modulo L. This convention ensures that each site interacts with its rightward and downward neighbors, and for $L > 2$ every undirected bond is counted exactly once.

At a given temperature T, the probability of observing a configuration $\mathbf{s}$ is governed by the Boltzmann distribution,

$$p(\mathbf{s}; T) = \frac{1}{Z}\, e^{-\beta E(\mathbf{s})},$$

where $E(\mathbf{s})$ is the energy of the configuration and

$$\beta = \frac{1}{k_B T},$$

is the *inverse temperature* with k_B as the Boltzmann constant. Adopting the Boltzmann distribution as our probability measure $p(\mathbf{s}; T)$ corresponds to describing the system in thermal equilibrium with its environment [3].

The normalization constant

$$Z = \sum_{\mathbf{s}} e^{-\beta E(\mathbf{s})}, \tag{4}$$

denotes the partition function, obtained by summing over all possible microstates $\mathbf{s}$. It essentially characterizes how the probability distribution over the state space shifts as the temperature T varies [4].

The total magnetization is obtained by summing over all spins,

$$M(\mathbf{s}) = \sum_{i=1}^{N} s_i. \tag{5}$$

As we are only interested in the degree of spin alignment rather than its orientation, we will use the absolute magnetization $|M|$ to quantify the strength of ordering in the system.[1]

The expectation values of key observables are defined as averages over all spin configurations, weighted by the Boltzmann distribution:

$$\langle E\rangle = \sum_{\mathbf{s}} E(\mathbf{s})\, p(\mathbf{s};T), \qquad \langle |M|\rangle = \sum_{\mathbf{s}} |M(\mathbf{s})|\, p(\mathbf{s};T),$$
$$\langle E^2\rangle = \sum_{\mathbf{s}} \Big(E(\mathbf{s})\Big)^2 p(\mathbf{s};T), \quad \langle M^2\rangle = \sum_{\mathbf{s}} \Big(M(\mathbf{s})\Big)^2 p(\mathbf{s};T),$$

where the sums extend over all possible microstates $\mathbf{s}$.

In practice, these quantities are estimated from Monte Carlo simulations by sampling raw energy and magnetization values. Statistical averages of energy, magnetization, heat capacity, and susceptibility then characterize the thermodynamic behavior of the system [5].

To enable meaningful comparison across lattices of different sizes, we report the *energy per spin* (ϵ) and the *magnetisation per spin* (m):

$$\epsilon(\mathbf{s}) = \frac{E(\mathbf{s})}{N}, \qquad m(\mathbf{s}) = \frac{M(\mathbf{s})}{N}.$$

Their expectation values follow directly,

$$\langle \epsilon\rangle = \frac{1}{N}\langle E\rangle, \qquad \langle |m|\rangle = \frac{1}{N}\langle |M|\rangle,$$
$$\langle \epsilon^2\rangle = \frac{1}{N^2}\langle E^2\rangle, \qquad \langle m^2\rangle = \frac{1}{N^2}\langle M^2\rangle.$$

Here, $\langle\epsilon\rangle$ and $\langle|m|\rangle$ quantify the mean energy per spin and the average degree of spin alignment, while the variances

$$\mathrm{Var}(\epsilon) = \langle\epsilon^2\rangle - \langle\epsilon\rangle^2, \quad \mathrm{Var}(m) = \langle m^2\rangle - \langle|m|\rangle^2,$$

measure the corresponding fluctuations. Together, these observables provide a concise statistical characterization of the system—its average energy content, the scale of its fluctuations, and the strength of spin ordering.

[1] In the absence of an external magnetic field, the expected magnetization $\langle M\rangle$ is always zero, since every spin configuration has an equally probable mirror state with all spins flipped. Using $|M|$ instead allows us to measure the strength of spin alignment, independent of orientation.

The heat capacity and magnetic susceptibility, normalized per spin, are defined as

$$\frac{C_V(T)}{N} = \frac{N}{k_B T^2}\Big(\langle\epsilon^2\rangle - \langle\epsilon\rangle^2\Big), \tag{6}$$
$$\frac{\chi(T)}{N} = \frac{N}{k_B T}\Big(\langle m^2\rangle - \langle|m|\rangle^2\Big). \tag{7}$$

Here, the heat capacity C_V quantifies fluctuations in the system's energy with temperature, while the magnetic susceptibility χ captures fluctuations in magnetization. Both exhibit pronounced peaks near the critical temperature, signaling collective behavior and the onset of phase transitions [6].

In the thermodynamic limit ($N \to \infty$), these quantities diverge at the critical temperature T_c, signaling a phase transition. For finite lattices, the divergence is replaced by sharp peaks near T_c, which sharpen and shift as the system size increases, revealing finite-size signatures of the transition. The Ising model therefore serves as a textbook example of a second-order phase transition, characterized by the divergence of both heat capacity and susceptibility [7].

Table I summarizes all units used throughout this project.

Quantity	**Symbol**	**Unit**
Spin variables	s_i	dimensionless
Energy	E	J
Energy per spin	ϵ	J
Temperature	T	J/k_B
Inverse temperature	β	$1/J$
Magnetization	M	dimensionless
Magnetization per spin	m	dimensionless
Coupling constant	J	J (energy)
Boltzmann constant	k_B	J/K
Heat capacity per spin	C_V/N	dimensionless
Susceptibility per spin	χ/N	dimensionless
Partition function	Z	dimensionless

TABLE I. Units used throughout the project. Energies are expressed in multiples of the coupling constant J. Temperatures are reported in energy units (J/k_B), consistent with the convention $k_B = 1$. Derived quantities such as heat capacity and susceptibility are normalized per spin, rendering them dimensionless.

B. The 2×2 Lattice

To build intuition, we begin with the simplest nontrivial case of the two-dimensional Ising model: the 2×2 lattice

$$\mathbf{s} = \begin{bmatrix} s_{1,1} & s_{1,2} \\ s_{2,1} & s_{2,2} \end{bmatrix},$$

with total number of spins $N = 4$. Consisting of only four sites the system admits $2^4 = 16$ distinct microstates. Such a small lattice permits explicit enumeration of all spin configurations and analytic evaluation of quantities such as the energy, magnetization, and partition function, which later serve to validate our numerical methods.

It should be noted that the 2×2 lattice constitutes a special case. Under periodic boundary conditions, each bond is effectively traversed twice, resulting in double-counting. This peculiarity contrasts with alternative boundary conditions, such as free ends, which we do not consider here.

Expanding (3) for $L = 2$ makes this explicit:

$$E(\mathbf{s}) = -2J\left(s_{1,1}\,s_{1,2} + s_{1,1}\,s_{2,1} + s_{1,2}\,s_{2,2} + s_{2,1}\,s_{2,2}\right).$$

Although the double-counting appears redundant, we retain it deliberately. This choice preserves the general form of the energy expression, avoids special-case rules for $L = 2$, and ensures consistency between analytical derivations and numerical implementations.

Using the definitions of the system energy (3) and total magnetization (5), we enumerate all 16 microstates of the 2×2 lattice under periodic boundary conditions. Table II groups these microstates into symmetry-equivalent classes, organized by energy and magnetization; the degeneracy column indicates the number of distinct spin configurations in each class. A complete enumeration of every microstate is provided in Appendix A.

j	# spins (↑)	E_j	M_j	d_j
1	4	-8	$+4$	1
2	3	0	$+2$	4
3	2 (adjacent)	0	0	4
4	2 (diagonal)	$+8$	0	2
5	1	0	-2	4
6	0	-8	-4	1

TABLE II. Distinct microstate classes j of the 2×2 Ising lattice under PBC. Energies E_j (in units of J) are computed with double-counted neighbor pairs. Magnetization M_j and degeneracy d_j are indicated; together the classes account for all 16 microstates.

We proceed to derive analytical expressions for the 2×2 lattice. To streamline notation, we introduce the dimensionless coupling

$$K \equiv \beta J.$$

Using Eq. (4) together with the degeneracies listed in Table II, the partition function can be explicitly evaluated:

$$\begin{aligned} Z &= \sum_{\mathbf{s}} e^{-\beta E(\mathbf{s})} = \sum_{j=1}^{6} d_j e^{-\beta E_j} \\ &= 2e^{8K} + 12e^{0} + 2e^{-8K} \\ &= 2e^{8K} + 2e^{-8K} + 12 \qquad (8) \\ &= 4\cosh(8K) + 12, \qquad (9) \end{aligned}$$

where the final step employs the identity $\cosh(x) = \frac{1}{2}\left(e^{x} + e^{-x}\right)$.

For brevity, the detailed derivations of the remaining expressions are relegated to Appendix B. From the partition function, the energy expectation values follow as:

$$\langle E\rangle = -\frac{16J}{Z}\left(e^{8K} - e^{-8K}\right), \qquad (10)$$

$$\langle \epsilon\rangle = -\frac{4J}{Z}\left(e^{8K} - e^{-8K}\right), \qquad (11)$$

$$\langle E^2\rangle = \frac{128J^2}{Z}\left(e^{8K} + e^{-8K}\right), \qquad (12)$$

$$\langle \epsilon^2\rangle = \frac{8J^2}{Z}\left(e^{8K} + e^{-8K}\right). \qquad (13)$$

Similarly, the magnetization expectation values can be expressed as:

$$\langle |M|\rangle = \frac{8}{Z}\left(e^{8K} + 2\right), \qquad (14)$$

$$\langle |m|\rangle = \frac{2}{Z}\left(e^{8K} + 2\right), \qquad (15)$$

$$\langle M^2\rangle = \frac{32}{Z}\left(e^{8K} + 1\right), \qquad (16)$$

$$\langle m^2\rangle = \frac{2}{Z}\left(e^{8K} + 1\right). \qquad (17)$$

Building on these, the heat capacity per spin is obtained from fluctuations in energy:

$$\frac{C_V}{N} = \frac{4}{k_B T^2}\left[\frac{8J^2}{Z}\left(e^{8K} + e^{-8K}\right) - \left(\frac{4J}{Z}\left(e^{8K} - e^{-8K}\right)\right)^2\right]. \qquad (18)$$

Finally, the magnetic susceptibility per spin is derived from magnetization fluctuations:

$$\frac{\chi}{N} = \frac{4}{k_B T}\left[\frac{1}{Z}\left(2e^{8K} + 2\right) - \left(\frac{1}{Z}\left(2e^{8K} + 4\right)\right)^2\right]. \qquad (19)$$

In summary, closed-form analytical expressions for the observables ϵ, C_V, m, and χ have been established for the 2×2 lattice.

C. Markov Chain Monte Carlo (MCMC)

Accurate sampling of the Boltzmann distribution becomes infeasible for systems with large configuration

space, such as an $L \times L$ Ising lattice containing 2^{L^2} possible spin configurations. Rather than enumerating all microstates, we employ a **Markov Chain Monte Carlo (MCMC)** method to generate a sequence of configurations whose long-time statistics reproduce the target equilibrium distribution $p(\mathbf{s}; T)$. In an MCMC scheme, the simulation proceeds through a Markov chain: each new configuration depends only on the current configuration, not on the full history of previous updates.

When the Markov chain is **ergodic** on a finite state space — that is, *irreducible* and *aperiodic*, so every configuration can be reached from any other in a finite number of steps, and there is no periodic structure — it admits a unique stationary distribution. If, in addition, the transition probabilities satisfy the **detailed balance** condition

$$p(\mathbf{s}; T)\, P(\mathbf{s} \to \mathbf{s}') = p(\mathbf{s}'; T)\, P(\mathbf{s}' \to \mathbf{s}),$$

with respect to the Boltzmann distribution, then the chain is time-reversible and $p(\mathbf{s}; T)$ is stationary. Ergodicity on a finite state space then guarantees that the distribution of the chain converges to $p(\mathbf{s}; T)$ from any initial state [8].

A single Monte Carlo update consists of two components:

1. Proposing a candidate configuration $\mathbf{s}'$ from the current configuration $\mathbf{s}$.
2. Accepting or rejecting this proposal according to a well-defined rule.

Each update adds another element to the sequence

$$\mathbf{s}^{(0)} \to \mathbf{s}^{(1)} \to \mathbf{s}^{(2)} \to \cdots$$

which constitutes the Markov chain. After a sufficient burn-in period, during which the chain loses memory of its initial configuration, ergodicity and detailed balance guarantee that long-time averages of observables converge to their equilibrium expectation values, even though successive samples are correlated [8, 9].

1. *Metropolis–Hastings and the Metropolis acceptance rule*

In this work we employ the **Metropolis algorithm**, a special case of the more general Metropolis–Hastings scheme. This algorithm begins by expressing the transition probability $P(\mathbf{s} \to \mathbf{s}')$ as the product of a proposal probability $T(\mathbf{s} \to \mathbf{s}')$ and an acceptance probability $A(\mathbf{s} \to \mathbf{s}')$:

$$P(\mathbf{s} \to \mathbf{s}') = T(\mathbf{s} \to \mathbf{s}')\, A(\mathbf{s} \to \mathbf{s}').$$

Given a current state $\mathbf{s}$, a new state $\mathbf{s}'$ is proposed according to T, and accepted with probability

$$A(\mathbf{s} \to \mathbf{s}') = \min\left(1,\ \frac{p(\mathbf{s}')}{p(\mathbf{s})}\right),$$

which is the Metropolis acceptance rule for a symmetric proposal.[2] For the Ising model, the Boltzmann probabilities reduce to ratios of exponentials

$$\frac{p(\mathbf{s}')}{p(\mathbf{s})} = \exp[-\beta(E(\mathbf{s}') - E(\mathbf{s}))] = \exp(-\beta \Delta E),$$

where the energy difference $\Delta E = E(\mathbf{s}') - E(\mathbf{s})$. The acceptance rule can then be written as

$$A(\mathbf{s} \to \mathbf{s}') = \begin{cases} 1, & \Delta E \le 0, \\ \exp(-\beta \Delta E), & \Delta E > 0, \end{cases} \tag{20}$$

meaning that energetically favorable moves are always accepted, while energetically unfavorable moves are accepted with a temperature-dependent probability. If a move is rejected, the chain remains in configuration $\mathbf{s}$. This dynamic ensures detailed balance and drives the Markov chain toward equilibrium while allowing the system to escape local minima [10].

In the Ising model, the proposal step consists of selecting a single spin uniformly at random and attempting to flip it,

$$s_{ij} \ \to \ -s_{ij}.$$

This single-spin-flip proposal is symmetric, since for any pair of configurations that differ by a single spin flip,

$$T(\mathbf{s} \to \mathbf{s}') = T(\mathbf{s}' \to \mathbf{s}),$$

and because any configuration can be reached from any other through a finite sequence of such flips, the dynamics are ergodic. With this symmetry, the detailed balance condition reduces to

$$p(\mathbf{s})\, A(\mathbf{s} \to \mathbf{s}') \ = \ p(\mathbf{s}')\, A(\mathbf{s}' \to \mathbf{s}),$$

so the Metropolis acceptance rule alone suffices to enforce detailed balance [10].

2. *General Monte Carlo iteration*

In the two-dimensional nearest-neighbour Ising model, only local interactions are affected by a single-spin flip, so the energy change ΔE can be evaluated efficiently and takes values from a small discrete set[3]:

$$\Delta E \in \{-8J,\ -4J,\ 0,\ 4J,\ 8J\}. \tag{21}$$

Consequently, for a fixed temperature T, only five distinct Boltzmann factors,

$$w(\Delta E) = e^{-\beta \Delta E},$$

---

[2] For notational simplicity we write $p(\mathbf{s})$ for the Boltzmann distribution at temperature T.

[3] A detailed derivation of these values is provided in Appendix C.

can appear in the simulation. To avoid repeatedly calling the expensive exponential function inside the inner Monte Carlo loop, we precompute these values once at the start of each simulation and store them in a lookup table $w(\Delta E)$. This improves efficiency while preserving the exact statistical properties of the Metropolis algorithm.

Algorithm 1 outlines the Metropolis update procedure:

Algorithm 1 Metropolis update for the Ising model

function METROPOLIS_UPDATE(**s**, L, $w(\Delta E)$)
  Choose random lattice site (i, j)
  Compute $\Delta E \leftarrow E_{\text{after}} - E_{\text{before}}$ for flipping $\mathbf{s}[i][j]$
  if $\Delta E \leq 0$ **then**
    Accept the flip
  else
    Draw $r \in [0, 1)$
    if $r < w(\Delta E)$ **then**
      Accept the flip
    else
      Reject the flip

3. Simulation protocol and sampling strategy

For each lattice size L and temperature T, we simulate an $L \times L$ Ising system using single–spin Metropolis updates at inverse temperature $\beta = 1/(k_B T)$, with $k_B = 1$. One Monte Carlo cycle is defined as $N = L^2$ attempted spin flips, so that on average each spin is offered a flip once per cycle. The Markov chain is advanced for n_{cycles} such cycles, and only the configuration at the end of each cycle is stored, which reduces storage requirements and mitigates correlations between successive recorded states. Because each proposal depends only on the current configuration, successive states are still correlated; recording observables once per Monte Carlo cycle corresponds to a modest amount of thinning that helps control autocorrelations without discarding an excessive amount of information [11].

A proposed flip with energy change ΔE is accepted with probability

$$w(\Delta E) = \min\{1, \exp(-\beta \Delta E)\}.$$

The first n_{burn} cycles are discarded as burn-in to allow equilibration, and observables are then accumulated and averaged over the remaining $n_{\text{meas}} = n_{\text{cycles}} - n_{\text{burn}}$ cycles to estimate $\langle \epsilon \rangle$, $\langle |m| \rangle$, C_V/N, and χ/N. Algorithm 2 summaries the simulation procedure, and the post–burn-in cycles constitute the ensemble of samples used in all subsequent analysis [12].

Algorithm 2 Ising MCMC simulation using Metropolis

function ISING_MCMC_SIMULATION(L, T, n_{cycles}, n_{burn}, **s**)
  $N \leftarrow L^2$
  $\beta \leftarrow 1/(k_B T)$ ▷ typically $k_B = 1$
  Precompute $w(\Delta E)$ ▷ $\Delta E \in \{-8J, -4J, 0, 4J, 8J\}$
  Initialize accumulators for ϵ, ϵ^2, $|m|$, m^2
  for $k = 1$ to n_{cycles} **do**
    for *step* $= 1$ to N **do**
      METROPOLIS_UPDATE(**s**, L, β, $w(\Delta E)$)
    if $k > n_{\text{burn}}$ **then**
      Compute $E(\mathbf{s})$ and $M(\mathbf{s})$
      Update sums for ϵ, ϵ^2, $|m|$, m^2
  Compute observables from accumulated sums
  return $\langle \epsilon \rangle$, $\langle |m| \rangle$, C_V/N, χ/N

D. Efficient Implementation of Periodic Boundary Conditions

A naive implementation of the Ising model checks whether a spin lies on the lattice boundary before accessing neighbors, leading to multiple `if`-tests in the innermost loops. This is inefficient and disrupts the regular control flow optimized by modern CPUs. Instead, we impose periodic boundary conditions using modulo index arithmetic.

For a two-dimensional lattice of size $L \times L$, sites are indexed by (i, j) with $i, j \in \{0, \ldots, L-1\}$. Nearest neighbors are obtained via

$$(i \pm 1 \bmod L,\ j), \qquad (i,\ j \pm 1 \bmod L),$$

so that boundary sites wrap around and each spin has exactly four neighbors. This eliminates branching logic in the Monte Carlo update loop.

In practice, each spin couples only to its right and down neighbors, with indices $(j+1) \bmod L$ and $(i+1) \bmod L$. This ensures every bond is counted once for $L > 2$, while periodicity is handled without `if`-conditions.

Algorithm 3 illustrates the resulting branch-free implementation of Eq. (3) for a general $L \times L$ lattice.

Algorithm 3 Ising lattice energy computation

function ISING_TOTAL_ENERGY_PBC(**s**, L)
  $E \leftarrow 0.0$
  for $i = 0$ to $L - 1$ **do**
    for $j = 0$ to $L - 1$ **do**
      $S \leftarrow \mathbf{s}[i][j]$
      $right \leftarrow \mathbf{s}[i][(j + 1) \bmod L]$
      $down \leftarrow \mathbf{s}[(i + 1) \bmod L][j]$
      $E \leftarrow E - S \cdot (right + down)$
  return E

E. Tools

Tools

The project was implemented in C++ using the Armadillo linear algebra library. Plots and figures were made using `matplotlib-cpp`. All code is available on our GitHub repository:
https://github.uio.no/erlinsa/fys3150-prj4.

ChatGPT

ChatGPT was used as a supplementary tool for LaTeX, C++ and python development, primarily aiding in debugging, generating boilerplate structures, and drafting the README. It also assisted with phrasing, spelling corrections and code documentation. In instances where we encountered conceptual or implementation challenges, we also consulted it for clarification and alternative approaches. It has also documented the code.

III. RESULTS AND DISCUSSION

A. Determining a Sufficient Number of Monte Carlo Cycles

To identify how many Monte Carlo cycles are necessary to obtain reliable estimates for the 2×2 Ising model at $T \in [1.0, 3.5]$, we examined how the sampled observables—in particular the mean energy per spin $\langle\epsilon\rangle$ and the mean absolute magnetization per spin $\langle|m|\rangle$—converged as the number of Monte Carlo cycles increased. A plot illustrating this behavior using $\Delta T = 0.01$ is shown in Fig. 3.

Because the 2×2 lattice contains only $2^4 = 16$ possible spin configurations, equilibration occurs very quickly. The simulation results show that runs with approximately 10^4 Monte Carlo cycles already yield values of $\langle\epsilon\rangle$ and $\langle|m|\rangle$ that agree with the exact analytic results to within about 10^{-3} (Fig. 4).

In addition to monitoring the raw convergence of the sampled observables, we also examined the relative error of the numerical results compared to the exact analytical values for the 2×2 lattice. As shown in Fig. 4, the relative error in the mean energy per spin,

$$\delta_\epsilon = \frac{|\langle\epsilon\rangle_{\mathrm{MC}} - \langle\epsilon\rangle_{\mathrm{exact}}|}{|\langle\epsilon\rangle_{\mathrm{exact}}|},$$

decreases rapidly as the number of Monte Carlo cycles increases. After approximately 10^4 cycles the relative error typically falls below 10^{-3}, and further increasing the simulation length yields diminishing improvements.

A similar behaviour is observed for the mean absolute

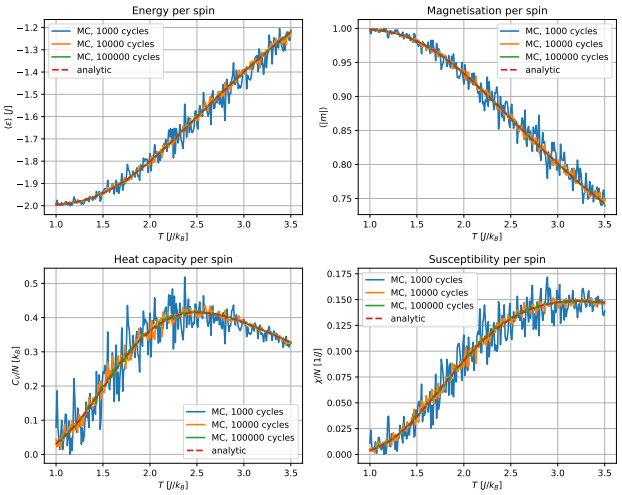

FIG. 3. Comparison of analytical and numerical results for $\langle\epsilon\rangle$, $\langle|m|\rangle$, C_V, and χ as functions of the temperature T with different number of Monte Carlo cycles. The system under consideration is a 2×2 spin lattice.

magnetisation per spin,

$$\delta_{|m|} = \frac{|\langle|m|\rangle_{\mathrm{MC}} - \langle|m|\rangle_{\mathrm{exact}}|}{\langle|m|\rangle_{\mathrm{exact}}}.$$

Because the analytic value of $\langle|m|\rangle$ for the 2×2 system is very close to unity, this observable also converges quickly: after about 10^4 Monte Carlo cycles the relative error again falls to the order of 10^{-3} or smaller.

At higher T, energy fluctuations increase, giving larger statistical uncertainty. The relative error decreases roughly *by about an order of magnitude each time the number of Monte Carlo cycles is increased by one order of magnitude*, indicating rapid convergence with simulation length.

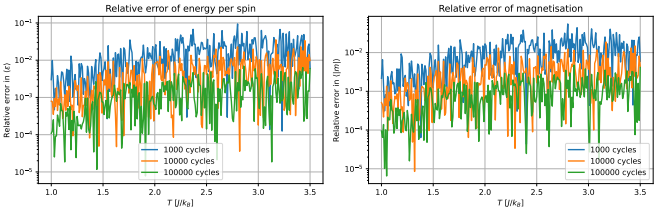

FIG. 4. Relative error between analytical and numerical results for $\langle\epsilon\rangle$, $\langle|m|\rangle$, as functions of the temperature T for a 2×2 spin lattice. The error decreases with increasing number of Monte Carlo cycles, illustrating convergence of the numerical estimates toward the analytical values. Generated with

B. Burn-in Behavior of the Metropolis Algorithm

To investigate the equilibration characteristics of the Metropolis algorithm, we studied the evolution of the in-

stantaneous energy per spin ϵ and its running average $\langle\epsilon\rangle$ as functions of Monte Carlo (MC) cycles for a 20×20 lattice. Figure 5 displays these quantities on a logarithmic cycle axis for two temperatures, $T = 1.0$ and $T = 2.4$, each simulated from both ordered and unordered initial configurations.

At both temperatures, the ordered initial state begins close to the equilibrium energy, while the unordered initial state starts significantly farther away. As the simulation progresses, the curves from the two initial conditions approach a common plateau, and the running averages flatten, indicating convergence toward stationarity. The equilibration behavior depends strongly on temperature: at $T = 2.4$ the trajectories relax rapidly, whereas at $T = 1.0$ the unordered initial configuration shows a prolonged drift before settling at the equilibrium value. The instantaneous energies (thin lines) fluctuate strongly, especially at the higher temperature, while the running averages (thick lines) effectively smooth out these fluctuations.

These observations allow us to identify the unordered low-temperature case as the slowest to equilibrate. This case therefore determines the necessary burn-in period for all subsequent measurements in later problems.

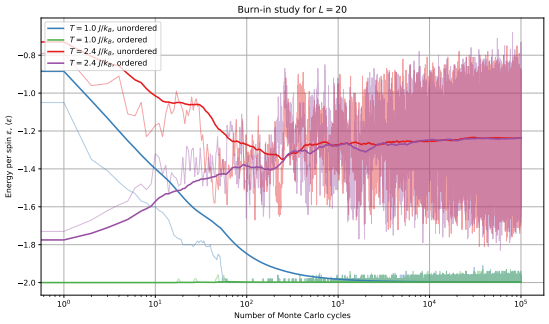

FIG. 5. Instantaneous energy per spin (thin lines) and running average energy per spin (thick lines) as functions of the number of Monte Carlo cycles for ordered and unordered initial conditions at $T = 1.0$ and $T = 2.4$. A logarithmic x-axis is used to resolve the early transient behaviour. Convergence of the trajectories from different initial states demonstrates that the system has reached equilibrium.

C. Energy distribution at low and high temperatures

To investigate thermal fluctuations of the Ising model, we generated the energy-per-spin samples ϵ for $L = 20$ at the temperatures $T = 1.0$ and $T = 2.4$ using the Metropolis Monte Carlo procedure with a burn-in of 50 000 cycles. The resulting normalized histograms are shown in Figure 6. These histograms provide an empirical estimate of the probability density $p_\epsilon(\epsilon; T)$.

At the low temperature $T = 1.0\,J/k_B$, the distribution is sharply peaked and narrow. The system is deep in the ordered phase, so only small thermal excitations occur and the sampled energies remain close to the ground-state value. Consequently, the variance of the distribution is very small: energy fluctuations are strongly suppressed because energetically costly spin flips are unlikely to be accepted.

At the higher temperature $T = 2.4\,J/k_B$, the distribution becomes significantly broader. This reflects the fact that the system, being close to the critical temperature $T_c \approx 2.269\,J/k_B$, undergoes large fluctuations in spin configurations. Many more microstates with widely varying energies are thermally accessible, leading to a much larger variance in ϵ. The increase in variance is directly connected to the increase in the heat capacity,

$$C_V = \frac{\langle E^2\rangle - \langle E\rangle^2}{k_B T^2},$$

which is known to peak near criticality. Our histogram therefore illustrates the expected physical behaviour: suppressed fluctuations in the low-temperature ordered phase and enhanced fluctuations in the near-critical regime.

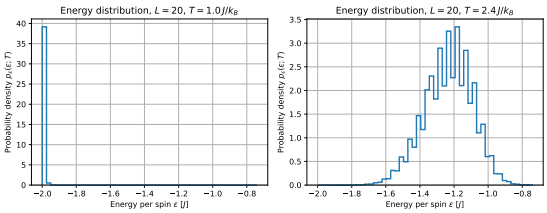

FIG. 6. Normalized histograms of the energy per spin ϵ for a 20×20 Ising lattice at $T = 1.0$ and $T = 2.4$. At low temperature the distribution is narrow and sharply peaked, indicating small thermal fluctuations in the ordered phase. Near the critical temperature the distribution broadens significantly, reflecting the large energy fluctuations expected in the near-critical regime.

D. Parallel performance of the OpenMP implementation

To investigate the parallel performance of our OpenMP-accelerated Ising model simulation, we measured the wall-clock time of the temperature loop using the C++ `std::chrono` high-resolution timer. The simulation was executed for lattice size $L = 2$, temperature range $T \in [1.0, 3.5]$ with 256 temperature points, and 10^6 Monte Carlo cycles per temperature. We varied the number of threads through the environment variable `OMP_NUM_THREADS`. The results are shown in Table III.

The results demonstrate near-linear scaling up to six threads, with a speedup of $S_6 \approx 5.43$ and efficiency of $E_6 \approx 0.90$, indicating excellent utilization of physical cores. At twelve threads, the speedup increases further to $S_{12} \approx 6.91$, but efficiency drops to $E_{12} \approx 0.58$, consistent

Threads p	Time T_p [s]	Speedup S_p	Efficiency E_p
1	34.049	1.00	1.00
6	6.275	5.43	0.90
12	4.929	6.91	0.58

TABLE III. Parallel performance of the OpenMP implementation. The table reports measured runtimes for different thread counts. From these values we compute the parallel speedup $S_p = T_1/T_p$ and efficiency $E_p = S_p/p$, illustrating how performance scales with the number of threads.

with expected limitations such as memory bandwidth saturation and thread management overhead. These findings confirm that the temperature sweep is an embarrassingly parallel task, requiring no synchronization between threads. Importantly, parallelization preserved the correctness and reproducibility of the simulation results. A plot of speedup and efficiency versus thread count (not shown here) would further illustrate the strong scaling behavior and the onset of diminishing returns beyond the number of physical cores.

E. Phase transition observables

Figure 7 shows the temperature dependence of the energy per spin, magnetization, heat capacity, and susceptibility for lattice sizes $L = 40, 60, 80$, and 100. The overall behavior is consistent with expectations for the two-dimensional Ising model near the critical point.

The energy decreases smoothly as the system orders at low temperature and shows only weak finite-size dependence. In contrast, the magnetization exhibits a rapid crossover from an ordered to a disordered state around $T \approx 2.27$–2.30. As L increases, this crossover becomes markedly sharper, reflecting the steepening of the order–disorder transition in the thermodynamic limit.

The heat capacity and susceptibility both exhibit pronounced peaks near the critical region. The susceptibility peak grows strongly with system size and shifts downward toward the Onsager critical temperature $T_c \approx 2.269$. The heat-capacity peak is broader and shows weaker size dependence, but its maximum also lies close to the critical region. From the peak locations we obtain the finite-size estimates

$$T_c^{(C_V)}(L) \approx 2.27\text{–}2.29, \qquad T_c^{(\chi)}(L) \approx 2.29\text{–}2.32,$$

which converge from above toward the exact value as L increases. The susceptibility systematically yields higher $T_c(L)$ than the heat capacity, which is expected: the susceptibility peak in finite systems typically occurs at a slightly higher temperature than the heat-capacity maximum due to rounding and the stronger divergence of χ [13, 14].

Overall, the results demonstrate the textbook finite-size behavior of the 2D Ising model. A potential improvement for future work would be to increase sampling near the peak region using adaptive temperature spacing or histogram reweighting. This would refine the peak locations and reduce statistical noise, particularly for the largest system sizes where computational cost is highest.

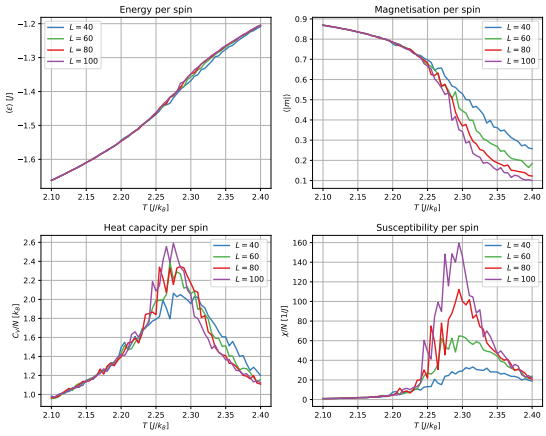

FIG. 7. Temperature dependence of the energy per spin, absolute magnetization, heat capacity per spin, and susceptibility per spin for lattice sizes $L = 40, 60, 80$, and 100. Each observable exhibits characteristic finite-size behavior near the critical temperature. The susceptibility peak sharpens and grows with increasing system size, while the heat capacity shows a broader peak with weaker size dependence. The magnetization transition becomes steeper as L increases, approaching the thermodynamic-limit behavior.

F. Finite-size scaling of the critical temperature

To estimate the thermodynamic-limit critical temperature $T_c(\infty)$, we extracted pseudocritical temperatures $T_c(L)$ from the maxima of the specific heat C_V/N and magnetic susceptibility χ/N for system sizes $L = 40, 60, 80$, and 100. Figure 8 shows $T_c(L)$ plotted as a function of $1/L$, together with linear fits based on the finite-size scaling relation

$$T_c(L) = T_c(\infty) + \frac{a}{L}.$$

Both observables exhibit a clear linear trend, indicating that the simple $1/L$ scaling ansatz captures the dominant finite-size behaviour in our simulations. Extrapolation of the fits to $1/L = 0$ yields

$$T_c(\infty) \approx 2.281 \quad \text{from } C_V/N, \qquad T_c(\infty) \approx 2.278 \quad \text{from } \chi/N.$$

These values differ by less than 0.5% from the exact Onsager value

$$T_c^{\text{exact}} = \frac{2}{\ln(1+\sqrt{2})} = 2.269185\ldots,$$

demonstrating that even with modest lattice sizes and a finite number of Monte Carlo cycles, the method provides a reliable estimate of the critical temperature.

The susceptibility-based estimate is slightly closer to the exact result, consistent with the fact that χ has a sharper peak than C_V, making the pseudocritical temperature easier to identify. Small deviations from perfect linearity are expected and likely arise from the finite temperature resolution of our sampling. A denser temperature grid or the use of histogram reweighting could improve the precision of the peak estimates.

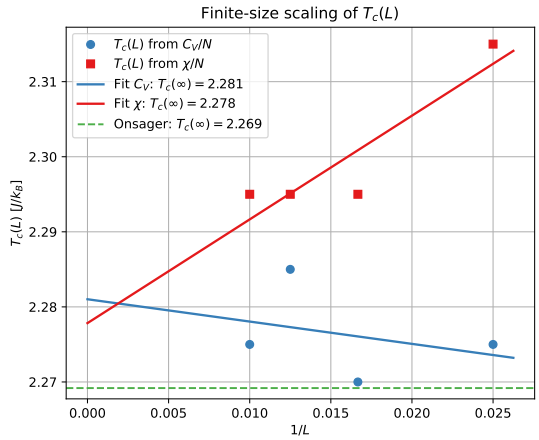

FIG. 8. Pseudocritical temperatures $T_c(L)$ extracted from the maxima of the heat capacity C_V/N and susceptibility χ/N, plotted against $1/L$. The straight-line fits correspond to the scaling form $T_c(L) = T_c(\infty) + a/L$, and the extrapolated intercepts give numerical estimates of the thermodynamic-limit critical temperature. The horizontal dashed line marks Onsager's exact value $T_c^{\text{exact}} = 2/\ln(1+\sqrt{2})$.

IV. CONCLUSION

In this project, we have explored the two-dimensional Ising model through analytical calculations, numerical simulations, and performance studies. We began by establishing the analytical baseline for the 2×2 system, then implemented a Markov Chain Monte Carlo algorithm to study larger lattices and compute key thermodynamic quantities. By validating our code, examining equilibration behavior, analyzing probability distributions, and investigating finite-size effects near the critical temperature, we gained both theoretical and computational insight into phase transitions in the 2D Ising model. These results demonstrate how numerical methods can successfully capture the statistical behavior of complex physical systems. In this section we summaries the main findings, limitations, and possible extensions of this work.

From the observations in section III A, we conclude that a simulation length of roughly 10^4 Monte Carlo cycles is sufficient to obtain stable and accurate thermodynamic averages for the 2×2 Ising system. Longer runs provide diminishing returns; for example, increasing the cycle count to 10^5 yields only minor improvements, reducing statistical fluctuations without significantly altering the mean values.

Both the energy and magnetization observables exhibit fast and systematic convergence, with relative errors typically falling below 10^{-3} after 10^4 cycles. This confirms that 10^4 Monte Carlo cycles strike an effective balance between computational efficiency and statistical reliability.

The burn-in analysis of Section III B demonstrates that the Metropolis algorithm requires a clear equilibration period before statistically reliable samples can be collected. Although all initial configurations eventually converge to the same equilibrium distribution, the unordered configuration at low temperature ($T = 1.0$) exhibits the slowest relaxation. As this represents the limiting case for equilibration, it sets the effective burn-in requirement for subsequent simulations. Based on the observed convergence behavior, discarding the first $\sim 10^4$ MC cycles is sufficient to ensure that the system has reached equilibrium and that only stationary samples contribute to the computed observables.

The analysis of the energy distributions in Section III C provides clear evidence of the temperature-dependent behavior of the two-dimensional Ising model. At low temperature the system remains close to the ground state, resulting in a narrow energy distribution with minimal variance. At higher temperature, particularly near the critical region, the distribution broadens and its variance increases substantially due to the large number of thermally accessible microstates and the enhanced fluctuations characteristic of criticality. These results are fully consistent with the theoretical expectations for the Ising model and further validate the correctness of our Monte Carlo implementation.

In Section III D we parallelized the temperature sweep of the Ising model simulation using OpenMP, exploiting its embarrassingly parallel structure. The runtime decreased from 34.0 s in serial execution to 6.3 s with six threads and 4.9 s with twelve threads, corresponding to speedups of 5.4 and 6.9. Efficiency remained high up to six threads ($\sim 90\%$), while the drop at twelve threads ($\sim 58\%$) reflects expected limits from memory bandwidth and oversubscription beyond physical cores.

Overall, OpenMP proved to be an effective and straightforward way to accelerate Monte Carlo simulations of the Ising model. Parallelizing over temperature values yields strong scaling, nearly an order-of-magnitude speedup, and substantial reductions in computational cost, all while preserving correctness and reproducibility.

The Monte Carlo simulations in Section III E successfully reproduce the expected finite-size signatures of the two-dimensional Ising phase transition. Both the magnetization curves and the diverging response functions (heat capacity and susceptibility) show clear sharpening with increasing system size, and the peak temperatures converge toward the exact critical temperature. The observed drift of $T_c(L)$ from above, especially in the susceptibility, is fully consistent with finite-size scaling the-

ory [13, 14].

Although the current results already capture the critical behavior clearly, further improvements could include higher-resolution temperature sampling, larger lattice sizes, or employing reweighting and variance-reduction techniques to obtain more accurate estimates of critical exponents. Nonetheless, the present study convincingly demonstrates the universal features of the 2D Ising model's phase transition.

Our finite-size scaling analysis in Section III F successfully reproduces the critical temperature of the two-dimensional Ising model with high accuracy. Both the C_V- and χ-based extrapolations yield values within 0.5% of the exact Onsager solution, confirming that relatively small lattices ($L \leq 100$) already contain sufficient information to extrapolate toward the thermodynamic limit. The linear $1/L$ scaling form provides a good approximation for the accessible system sizes, though higher-order corrections could be resolved through larger lattices, finer temperature sampling, or more sophisticated peak-finding techniques.

Overall, the results demonstrate that the implemented Metropolis algorithm, combined with finite-size scaling, forms a robust framework for studying critical behavior in the 2D Ising model.

Appendix A: Microstates of the 2×2 Ising Model

A complete enumeration of all 16 microstates of the 2×2 lattice is provided in Table IV.

k	$\mathbf{s}_k$	E_k	M_k
1	$[+1,+1,+1,+1]$	-8	+4
2	$[+1,+1,+1,-1]$	0	+2
3	$[+1,+1,-1,+1]$	0	+2
4	$[+1,+1,-1,-1]$	0	0
5	$[+1,-1,+1,+1]$	0	+2
6	$[+1,-1,+1,-1]$	0	0
7	$[+1,-1,-1,+1]$	+8	0
8	$[+1,-1,-1,-1]$	0	-2
9	$[-1,+1,+1,+1]$	0	+2
10	$[-1,+1,+1,-1]$	+8	0
11	$[-1,+1,-1,+1]$	0	0
12	$[-1,+1,-1,-1]$	0	-2
13	$[-1,-1,+1,+1]$	0	0
14	$[-1,-1,+1,-1]$	0	-2
15	$[-1,-1,-1,+1]$	0	-2
16	$[-1,-1,-1,-1]$	-8	-4

TABLE IV. All 16 microstates of a 2×2 Ising model (PBC). Configurations are written in square brackets $[a, b, c, d]$, denoting row-major 2×2 matrices with the first two entries forming the top row and the last two the bottom row. Results show $E_k \in \{-8, 0, +8\}$ in units of J, and magnetization M is unitless.

Appendix B: Analytical Derivations for the 2×2 Ising System

Appendix B is currently a work in progress. Additional effort is needed to refine the references and overall presentation. Due to time constraints, further polishing will be undertaken—if there is still time—once the main body of the report has been completed.

Building on the spin configurations summarized in Table II, and recalling that the system size is $N = 4$, we now derive the full set of analytical expressions for the 2×2 Ising lattice. To maintain clarity, we continue to use the dimensionless coupling constant $K \equiv \beta J$. The partition function Z is given in Eq. (8) and Eq. (9). We make use of the definitions of the hyperbolic functions

$$\cosh(x) = \frac{e^x + e^{-x}}{2}, \qquad \sinh(x) = \frac{e^x - e^{-x}}{2}.$$

Expectation value of the energy

$$\begin{aligned}\langle E \rangle &= \frac{1}{Z} \sum_j d_j E_j e^{-\beta E_j} \\ &= \frac{1}{Z} \left[(-8J) \cdot 2e^{8K} + (8J) \cdot 2e^{-8K} \right] \\ &= -\frac{16J}{Z} \left(e^{8K} - e^{-8K} \right) \\ &= -\frac{32J}{Z} \sinh(8K).\end{aligned}$$

The energy per spin expectation value

$$\begin{aligned}\langle \epsilon \rangle = \frac{\langle E \rangle}{N} &= -\frac{4J}{Z} \left(e^{8K} - e^{-8K} \right) \\ &= -\frac{8J}{Z} \sinh(8K).\end{aligned}$$

The squared energy expectation value

$$\begin{aligned}\langle E^2 \rangle &= \frac{1}{Z} \sum_j d_j E_j^2 e^{-\beta E_j} \\ &= \frac{1}{Z} \left[(64J^2) \cdot 2e^{8K} + (64J^2) \cdot 2e^{-8K} \right] \\ &= \frac{128J^2}{Z} \left(e^{8K} + e^{-8K} \right) \\ &= \frac{256J^2}{Z} \cosh(8K).\end{aligned}$$

The squared energy per spin expectation value

$$\begin{aligned}\langle \epsilon^2 \rangle = \frac{\langle E^2 \rangle}{N^2} &= \frac{8J^2}{Z}\left(e^{8K} + e^{-8K}\right) \\ &= \frac{16J^2}{Z}\cosh(8K).\end{aligned}$$

The absolute magnetization expectation value

$$\begin{aligned}\langle |M| \rangle &= \frac{1}{Z}\left[4 \cdot 2e^{8K} + 2 \cdot 8 \cdot 1\right] \\ &= \frac{1}{Z}\left(8e^{8K} + 16\right) \\ &= \frac{8}{Z}\left(e^{8K} + 2\right).\end{aligned}$$

The absolute magnetization per spin expectation value

$$\langle |m| \rangle = \frac{\langle |M| \rangle}{N} = \frac{1}{Z}\left(2e^{8K} + 4\right) = \frac{2}{Z}\left(e^{8K} + 2\right).$$

The squared magnetization expectation value

$$\begin{aligned}\langle M^2 \rangle &= \frac{1}{Z}\left[16 \cdot 2e^{8K} + 4 \cdot 8 \cdot 1\right] \\ &= \frac{1}{Z}\left(32e^{8K} + 32\right) \\ &= \frac{32}{Z}\left(e^{8K} + 1\right).\end{aligned}$$

The squared magnetization per spin expectation value

$$\begin{aligned}\langle m^2 \rangle = \frac{\langle M^2 \rangle}{N^2} &= \frac{1}{16Z}\left(32e^{8K} + 32\right) \\ &= \frac{1}{Z}\left(2e^{8K} + 2\right) \\ &= \frac{2}{Z}\left(e^{8K} + 1\right).\end{aligned}$$

The heat capacity per spin

Using the following equation

$$\frac{C_V(T)}{N} = N\,\frac{1}{k_B T^2}\left[\langle \epsilon^2 \rangle - \langle \epsilon \rangle^2\right].$$

Insert $\langle \epsilon \rangle$ and $\langle \epsilon^2 \rangle$:

$$\begin{aligned}\frac{C_V}{N} &= \frac{4}{k_B T^2}\left[\frac{8J^2}{Z}\left(e^{8K} + e^{-8K}\right) - \left(\frac{4J}{Z}\left(e^{8K} - e^{-8K}\right)\right)^2\right] \\ &= \frac{4}{k_B T^2}\left[\frac{16J^2}{Z}\cosh(8K) - \left(\frac{8J}{Z}\sinh(8K)\right)^2\right] \\ &= \frac{4}{k_B T^2}\left[\frac{16J^2}{Z}\cosh(8K) - \frac{64J^2}{Z^2}\sinh^2(8K)\right] \\ &= \frac{64J^2}{k_B T^2}\left[\frac{\cosh(8K)}{Z} - \frac{4\sinh^2(8K)}{Z^2}\right].\end{aligned}$$

The magnetic susceptibility per spin

Using the following equation

$$\frac{\chi(T)}{N} = N\,\frac{1}{k_B T}\left[\langle m^2 \rangle - \langle |m| \rangle^2\right].$$

Insert $\langle m^2 \rangle$ and $\langle |m| \rangle^2$:

$$\begin{aligned}\frac{\chi}{N} &= \frac{4}{k_B T}\left[\frac{1}{Z}\left(2e^{8K} + 2\right) - \left(\frac{1}{Z}\left(2e^{8K} + 4\right)\right)^2\right] \\ &= \frac{4}{k_B T}\left[\frac{2}{Z}\left(e^{8K} + 1\right) - \frac{4}{Z^2}\left(e^{8K} + 2\right)^2\right].\end{aligned}$$

Appendix C: Energy change for a single spin flip

In the Metropolis update (Section II C 2), a proposed move consists of flipping a single spin on the lattice,

$$s_{i,j} \longrightarrow -s_{i,j}.$$

Only the terms in the Hamiltonian involving this spin can change the total energy. Using the energy expression from Eq. (3), each spin interacts with its four nearest neighbors: left, right, up, and down. For compactness, define the neighbor sum

$$S_{i,j} \equiv s_{i,j+1} + s_{i,j-1} + s_{i+1,j} + s_{i-1,j}.$$

The part of the energy involving $s_{i,j}$ before the flip is

$$E_{\text{local}} = -J\, s_{i,j}\, S_{i,j}.$$

After the flip $s'_{i,j} = -s_{i,j}$, the corresponding contribution becomes

$$E'_{\text{local}} = -J\,(-s_{i,j})\, S_{i,j} = +J\, s_{i,j}\, S_{i,j}.$$

Thus the spin-flip energy change is

$$\Delta E = E'_{\text{local}} - E_{\text{local}} = 2J\, s_{i,j}\, S_{i,j}. \tag{C1}$$

Since each neighbor takes values ± 1, a spin in a lattice with $L > 2$ has four distinct neighbors. Thus,

$$S_{i,j} \in \{-4, -2, 0, 2, 4\}.$$

Since $s_{i,j} = \pm 1$, the product $s_{i,j}S_{i,j}$ also lies in this set. Substituting into Eq. (C1), we obtain

$$\Delta E \in \{-8J,\, -4J,\, 0,\, 4J,\, 8J\}, \tag{C2}$$

showing that only five distinct energy changes can occur for a single spin flip.

For the special case $L = 2$, periodic boundaries cause each spin to have only two *unique* neighbors, each counted twice in the Hamiltonian. Consequently,

$$S_{i,j} \in \{-4, 0, 4\}, \qquad \Delta E \in \{-8J, 0, 8J\}.$$

This quirk, however, is more of an analytical detail than a coding problem.

In summary, under periodic boundary conditions with $L > 2$, a single spin flip can alter the energy by only five discrete values. This observation is essential for optimizing the Metropolis algorithm.

[1] Anders Kvellestad. FYS3150 - Lecture Notes. https://github.com/anderkve/FYS3150/blob/master/lecture_notes/2025/lecture_notes.pdf, 2025. Version 1.18.1, page 161. Accessed on November 07, 2025.

[2] Morten Hjorth-Jensen. Computational Physics. https://github.com/CompPhysics/ComputationalPhysics/blob/master/doc/Lectures/lectures2015.pdf, 2015. Page 421-422. Accessed on November 10, 2025.

[3] Anders Kvellestad. FYS3150 - Lecture Notes. https://github.com/anderkve/FYS3150/blob/master/lecture_notes/2025/lecture_notes.pdf, 2025. Version 1.18.1, page 164. Accessed on November 10, 2025.

[4] Anders Kvellestad. FYS3150 - Lecture Notes. https://github.com/anderkve/FYS3150/blob/master/lecture_notes/2025/lecture_notes.pdf, 2025. Version 1.18.1, page 165. Accessed on November 11, 2025.

[5] Anders Kvellestad. FYS3150 - Lecture Notes. https://github.com/anderkve/FYS3150/blob/master/lecture_notes/2025/lecture_notes.pdf, 2025. Version 1.18.1, page 165-167. Accessed on November 11, 2025.

[6] Anders Kvellestad. FYS3150 - Project 4. https://anderkve.github.io/FYS3150/book/projects/project4.html#problem-1, 2025. Accessed on November 15.

[7] Morten Hjorth-Jensen. Computational Physics. https://github.com/CompPhysics/ComputationalPhysics/blob/master/doc/Lectures/lectures2015.pdf, 2015. Page 430-431. Accessed on November 11, 2025.

[8] Anders Kvellestad. FYS3150 - Lecture Notes. https://github.com/anderkve/FYS3150/blob/master/lecture_notes/2025/lecture_notes.pdf, 2025. Version 1.18.1, page 151-153. Accessed on November 17, 2025.

[9] Anders Kvellestad. FYS3150 - Lecture Notes. https://github.com/anderkve/FYS3150/blob/master/lecture_notes/2025/lecture_notes.pdf, 2025. Version 1.18.1, page 157-158. Accessed on November 17, 2025.

[10] Anders Kvellestad. FYS3150 - Lecture Notes. https://github.com/anderkve/FYS3150/blob/master/lecture_notes/2025/lecture_notes.pdf, 2025. Version 1.18.1, page 153-156. Accessed on November 16, 2025.

[11] Anders Kvellestad. FYS3150 - Lecture Notes. https://github.com/anderkve/FYS3150/blob/master/lecture_notes/2025/lecture_notes.pdf, 2025. Version 1.18.1, page 158-160. Accessed on November 17, 2025.

[12] Anders Kvellestad. FYS3150 - Lecture Notes. https://github.com/anderkve/FYS3150/blob/master/lecture_notes/2025/lecture_notes.pdf, 2025. Version 1.18.1, page 167-169. Accessed on November 18, 2025.

[13] Morten Hjorth-Jensen. Computational Physics. https://github.com/CompPhysics/ComputationalPhysics/blob/master/doc/Lectures/lectures2015.pdf, 2015. Page 429-432. Accessed on November 17, 2025.

[14] Anders Kvellestad. FYS3150 - Project 4 - Problem 9 - Theoretical Background. https://anderkve.github.io/FYS3150/book/projects/project4.html#problem-9, 2025. Accessed on November 18.